Journal of Applied Physics

Structural and electronic properties of monodomain ultrathin $PbTiO_3/SrTiO_3/PbTiO_3/SrRuO_3$ heterostructures: A first-principles approach

Cite as: J. Appl. Phys. **128**, 244102 (2020); https://doi.org/10.1063/5.0031505
Submitted: 06 October 2020 . Accepted: 03 December 2020 . Published Online: 22 December 2020

Reza Mahjoub, Valanoor Nagarajan, and Javier Junquera

Journal of Applied Physics ARTICLE scitation.org/journal/jap

Structural and electronic properties of monodomain ultrathin $PbTiO_3/SrTiO_3/PbTiO_3/SrRuO_3$ heterostructures: A first-principles approach

Cite as: J. Appl. Phys. **128**, 244102 (2020); doi: 10.1063/5.0031505
Submitted: 6 October 2020 · Accepted: 3 December 2020 ·
Published Online: 22 December 2020

Reza Mahjoub,[1,a)] Valanoor Nagarajan,[2] and Javier Junquera[3]

AFFILIATIONS

[1]Future Industry Institute, University of South Australia, Mawson Lakes, SA 5095, Australia
[2]School of Materials Science and Engineering, The University of New South Wales (UNSW Sydney), Sydney, NSW 2052, Australia
[3]Departamento de Ciencias de la Tierra y Física de la Materia Condensada, Universidad de Cantabria, Cantabria Campus Internacional, Avenida de los Castros s/n, 39005 Santander, Spain

Note: This paper is part of the Special Topic on Domains and Domain Walls in Ferroic Materials.
a)Author to whom correspondence should be addressed: Reza.Mahjoub@unisa.edu.au

ABSTRACT

First-principles calculations within the local density approximation were carried out to explain the ground state and electronic properties of a vacuum/$PbTiO_3/SrTiO_3/PbTiO_3/SrRuO_3$ multilayer in a monodomain phase. Open-circuit boundary conditions were assumed, considering the electric displacement field, D, as the fundamental electrical variable. The direction and the magnitude of D can be monitored by proper treatment of the PbO surface layer, introducing external fractional charges Q in the surface atomic layers by means of virtual crystal approximation. Different excess or deficit surface charges (from $Q = \pm 0.05$ to $Q = \pm 0.15$) were considered, corresponding to small values of the polarization (up to $\pm 0.16\,C/m^2$) in both directions. The layer-by-layer electric polarization, tetragonality, and the profile of the electrostatic potential were computed, as well as the projected density of states, as a function of electric displacement field. The magnitude of D is preserved across the dielectric layers, which translates into a polarization of the $SrTiO_3$ spacer layer. The tetragonality of the two $PbTiO_3$ layers is different, in good agreement with experimental x-ray diffraction techniques, with the layer closer to the free surface exhibiting a smaller value. This is attributed to the interplay with surface effects that tend to contract the material in order to make the remaining bonds stronger. Our calculations show how the final structure in this complex oxide heterostructure comes from a delicate balance between electrical, mechanical, and chemical boundary conditions.

I. INTRODUCTION

It is well established that epitaxial heterostructures comprising ultrathin perovskite layers may present emergent properties, which may be absent in their individual constituents.[1–3] Among the immense number of possible combinations between ABO_3 perovskite oxides, $(PbTiO_3)_n/(SrTiO_3)_m$ superlattices (where n and m are, respectively, the number of unit cells of each perovskite combined in the heterostructure) have received significant interest during the last few years. Different ground states with a large variety of functional properties can be accessed by simply playing with the periodicity, layer sequence at the heterostructures, the strain conditions imposed by the substrate, the temperature,[4] or the electric field[5] applied between two external electrodes. Even, in ultrashort period superlattices ($n = m = 1$), the emergence of an improper ferroelectricity has been reported.[6] For larger periodicities, a transition between an electrostatically coupled regime (for small enough values of n and m) to an electrostatically decoupled regime (for larger values of n) has been theoretically predicted[7,8] and experimentally characterized.[9] The driving force for this transition is the depolarizing field: the divergence of the polarization

(i.e., any discontinuity in the out-of-plane component of the polarization) at the interface between the $PbTiO_3$ and $SrTiO_3$ yields to polarization charges, responsible for large electric fields that oppose the polarization and are electrostatically very costly. For thin enough periodicities, the electrostatic energy penalty due to the coupling of the depolarizing field and the polarization is alleviated by adopting a state of uniform out-of-plane polarization (without any discontinuity) in a monodomain configuration throughout the heterostructure.[7,8] Within this scenario, the value of the polarization, tetragonality, and transition temperature for the ferroelectric/paraelectric transition depends on the relative fraction of the ferroelectric layer and on the mechanical boundary conditions.[10] For thicker periodicities, the system forms a polydomain structure, with the polarization confined within the ferroelectric layers, to eliminate the depolarization fields and lower the total energy of the superlattice. The crossover between the two regimes was estimated to be around $n = m = 3 - 4$ unit cells,[9] smaller than the critical periodicity of $n = m = 7$ unit cells observed for the related $KNbO_3/KTaO_3$ ferroelectric/dielectric superlattices.[11] Despite this simple characterization, the real situation is more nuanced: the interplay between mutual interlayer strains and the electrostatics demanding the continuity of the out-of-plane displacement field leads to complex polarization rotation patterns and unusual domain structures, including the formation of clockwise/counterclockwise vortices[12] with exotic properties like the presence of regions with local negative capacitance,[13,14] chirality, and large circular dichroism,[15] or the appearance of topological bubble domains[16,17] and skyrmionic phases.[18]

The depolarizing field has been traditionally seen as detrimental for the functional properties of the superlattices, mostly based on the existence of an homogeneous polarization state. However, some recent works have suggested that it can have a positive role on the behavior of ultrathin ferroelectric films[19,20] as it is the main driving force behind the rich phase diagrams. Different works have proposed that the depolarization field can be considered as another degree of freedom to play with in the determination of the ground state and have suggested ways to tune it in ferroelectric $PbTiO_3$/metallic electrode heterostructures. For instance, introducing $SrTiO_3$ layers in between the electrode and $PbTiO_3$ thin films,[19] the dielectric spacer increases the effective screening length of the electrode and can be used to induce polydomain bubble states in originally monodomain structures, and thereby enhance dielectric properties of the ferroelectric thin films through the contribution of large domain walls to dielectric permittivity. If the $SrTiO_3$ spacer is introduced not between the ferroelectric thin film and the electrode, but inserted in the middle of the ferroelectric layer, then it causes 180° polydomain phase transition in the as grown state, thereby yielding significant improvement of dielectric leakage and marked reduction of the imprint.[20]

In the former experimental works, a direct visualization of the structure with atomic resolution to discriminate between monodomain and polydomain phases is not always possible. The polarization state of the different layers of the ferroelectric and the dielectric has to be indirectly inferred from fitting the x-ray diffraction peaks to some numerical models,[21] taking the number of unit cells of each material and the lattice parameters as the independent variables. Moreover, the actual value of the polarization is not accessible from these experiments, and phenomenological models can only provide qualitative answers.[20] Those are the questions we have addressed in this work. Going beyond the previous models[20] in this system, here we report first-principles simulations on the structural and electronic properties of a 14 unit cell $PbTiO_3$ thin film grown on a $SrRuO_3$ metallic electrode where, following the spirit of the previous experiments, a spacing layer of three unit cells of $SrTiO_3$ has been intentionally introduced at the center of the ferroelectric. A full relaxation of the structure would induce a Schottky breakdown and the pathological population of the bottom of the conduction band of the ferroelectric due to the underestimation of its bandgap.[22] Therefore, we work under open-circuit boundary conditions and fix the macroscopic displacement field (roughly the same as the polarization within the ferroelectric). The explored polarization states would correspond to the values expected close to the critical temperature into the homogeneous ferroelectric phase ($T_{\uparrow\uparrow}$ in the notation of Ref. 23). Our computations are able to reproduce a key experimental result, that is, the tetragonality of the two ferroelectric $PbTiO_3$ layers is significantly different. In accordance with previous experiments, the layer closer to the free surface assumes a smaller value due to depolarization field induced surface relaxation effects. Furthermore, these are only possible when the $SrTiO_3$ layer is polarized to minimize the electrostatic energy. Again, this is in perfect agreement with the experimental results.

The paper is organized as follows: in Sec. II, we describe the technicalities of our simulations, including the recipe to fix the value of the electric displacement field using fractional external charges. In Sec. III, we present the results, making emphasis on the atomic structure (Sec. III A) and in the electronic structure (Sec. III B) of our slabs. Finally, in Sec. IV, we present our conclusions and outlook for future research.

II. METHODS

We have carried out first-principles simulations based on the local density approximation (LDA)[24] to the density functional theory (DFT),[25,26] as implemented in the SIESTA code.[27] Core electrons were replaced by *ab initio* norm conserving pseudopotentials, generated using the Troullier–Martins scheme[28] in the Kleinman–Bylander fully non-local separable representation.[29] The one-electron Kohn–Sham eigenstates were expanded in a basis of strictly localized numerical atomic orbitals.[30,31] All the details of the pseudopotentials and basis sets can be found in Ref. 32 (for Sr, Ti, and O), Ref. 33 (for Pb), and in the supplementary material of Ref. 34 (for Ru).

For the Brillouin zone integrations, we used a Monkhorst–Pack sampling[35] equivalent to $6 \times 6 \times 6$ in a five-atom perovskite unit cell. A Fermi–Dirac distribution was chosen for the occupation of the one-particle Kohn–Sham electronic eigenstates with a smearing temperature of 0.075 eV (870 K). The electronic density, Hartree, and exchange-correlation potentials, as well as the corresponding matrix elements between the basis orbitals were computed on a uniform real space grid with an equivalent plane-wave cutoff of 500 Ry in the representation of the charge density.

To simulate the heterostructure, we used a tetragonal (1×1) supercell, periodically repeated in space, of the type vacuum/$(PbTiO_3)_7/(SrTiO_3)_3/(PbTiO_3)_7/(SrRuO_3)_{5.5}$, as shown in Fig. 1.

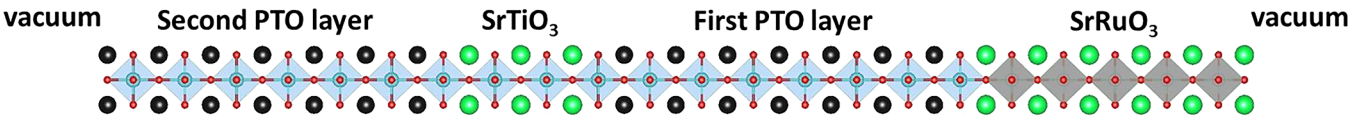

FIG. 1. Schematic representation of the supercell used in this work. Atoms are represented by spheres: Pb in black, Sr in green, Ru in gray, Ti in blue, and O in red with the oxygen octahedra colored accordingly to the B-cation at the center. In the remaining of this work, the $PbTiO_3$ layer in between the $SrRuO_3$ metallic electrode and the $SrTiO_3$ spacer layer will be referred to as the first-$PbTiO_3$ layer, and the $PbTiO_3$ region between vacuum and $SrTiO_3$ as the second-$PbTiO_3$ layer.

The periodicities correspond with the structures experimentally grown in Ref. 20. Free surfaces were terminated with a PbO layer on the $PbTiO_3$ side since this is the only stable surface termination found by first-principles[36] and with a SrO layer on the $SrRuO_3$ side due to the volatility of Ru. In order to simulate the effect of the mechanical boundary conditions due to the strain imposed by an hypothetical substrate, the in-plane lattice constant was fixed to the theoretical equilibrium lattice constant of bulk $SrTiO_3$ ($a_0 = 3.874$ Å), one of the most common substrates used to grow oxide heterostructures. The free PbO surface is modified to control the macroscopic electric displacement as explained below. As the starting point, an ideal structure was defined stacking along the [001] direction, the corresponding number of unit cells of $SrTiO_3$, $PbTiO_3$, and $SrRuO_3$ assuming a bulk centrosymmetric configuration, subject to the previous strain. The (1×1) periodicity in the plane inhibits the formation of domains in the simulations, and, therefore, all the calculations have been performed assuming a monodomain configuration. The vacuum thickness was equivalent to roughly ten unit cells of the perovskite. A dipole correction was introduced to avoid spurious interaction between periodic images of the slab in the out-of-plane direction.[37,38] A conjugate gradient minimization was performed till the maximum component of the force on any atom was smaller than 0.05 eV/Å.

Once the atomic structure is relaxed and the one-particle density matrix converged, in order to compute the density of states, a non-self-consistent calculation was carried out with a much denser sampling of $60 \times 60 \times 2$ Monkhorst–Pack mesh.

To perform simulations where the normal component of the displacement field is the independent input variable, we introduce a layer of external fractional charges (Q per surface unit cell S)[39] at the free surface of the vacuum/ferroelectric/metal superlattice, as suggested in Refs. 22 and 40. Since we enforce that the macroscopic electric field in vacuum is strictly zero (due to the use of the dipolar slab correction), if the surfaces remain locally insulating at electrostatic equilibrium (a vanishing density of states at the Fermi energy), then the continuity of the normal component of the macroscopic electric displacement imposes that

$$D = \frac{Q}{S}. \tag{1}$$

In practice, the external fractional charge is introduced making use of the virtual crystal approximation.[41,42] Using "alchemical" atoms, whose pseudopotential is a mixture of oxygen and fluorine or nitrogen, we can include in our simulation atoms with a fractional nuclear charge. If the percentage of F (respectively, N) in the mixture is Q, then the fictitious atom will have a fractional ionic charge of $Z = 8 + Q$ (respectively, $Z = 8 - Q$), and the nominal static charge will amount to $Z^{\text{nominal}}_{O_{(1-Q)}F_Q} = -2 + Q$, respectively ($Z^{\text{nominal}}_{O_{(1-Q)}N_Q} = -2 - Q$). Therefore, the individual layer at the free surface (composed by a Pb atom and the alchemical atom) has a formal surface charge density of Q/S (respectively, $-Q/S$). Here in this work, we have carried out simulations at $Q = \pm 0.05$, $Q = \pm 0.10$, and $Q = \pm 0.15$. This method presents two advantages with respect the original one devised by Stengel and co-workers in Ref. 43 that relied on the direct application of macroscopic electric fields. First, it can be used for metallic systems. Second, it nicely adopts to the standard computational techniques available in any standard computational package, as the one used in the present work.

To establish the notation, we shall call the plane-parallel to the interface (x, y) plane, whereas the perpendicular direction will be referred to as the z axis. Unless otherwise stated, all the physical quantities refer to the corresponding component along this z-direction. We shall use atomic units ($|e| = \hbar = m_e = 1$) throughout this work.

III. RESULTS

A. Atomic structure

In order to characterize the atomic displacements induced by the relaxation, we define $\delta_z(M_i)[\delta_z(O_i)]$ as the displacement of the cation [oxygen] along z at layer i with respect to the initial *reference* configuration. We introduce the displacement of the mean position of each atomic plane as $\beta_i = [\delta_z(M_i) + \delta_z(O_i)]/2$ and the change in the interplanar distance between consecutive planes i and j as $\Delta d_{ij} = \beta_i - \beta_j$. Then, the tetragonality of a given unit cell centered on layer i is computed adding the interplanar distance with respect to the neighboring layers (at the top and at the bottom) and dividing by the in-plane lattice constant a_0. The rumpling parameter of layer i describes the movement of the ions with respect to the mean position of each atomic plane and corresponds to $\eta_i = [\delta_z(M_i) - \delta_z(O_i)]/2$. It is positive when the cation M_i is above the oxygen and negative otherwise.

The local polarization is obtained calculating the polarization of a unit cell centered on every cation of the system (except at the interfaces where no "bulklike" unit cell can be chosen), and using the displacement of the atoms with respect to the ideal phase and the Born-effective charges obtained for the bulk tetragonal centrosymmetric phase of the corresponding strained material, either $PbTiO_3$ or $SrTiO_3$, depending on the layer, the cation belongs to. They have been renormalized, following the recipe given in Ref. 22,

in order to take into account that the Born-effective charges are computed under zero macroscopic electric field, but here we are computing the layer polarization under a given macroscopic electric displacement (i.e., the electric field might be different from zero). In practice, this translates into the fact that the layer-by-layer polarization is rescaled by a factor of 0.93 for $PbTiO_3$.

The layer-by-layer polarization, rumpling, tetragonality, and the profile of the smoothed electrostatic potential are plotted in Fig. 2 for a slab with $Q = \pm 0.10e$, which translates into a macroscopic displacement field of $D = 1.866 \times 10^{-3}\,\mathrm{e/bohr^2} = 0.107\,\mathrm{C/m^2}$. Similar results (not shown) are obtained for values of the external fractional charge of $Q = \pm 0.05$. Several conclusions can be drawn from Fig. 2. First of all, we can see how both $PbTiO_3$ and $SrTiO_3$ are polarized with a local value of the polarization [Fig. 2(a)] that roughly equals the imposed value of electric displacement field D. Indeed, the approximation of the local electric displacement $D(z)$ with the local polarization $P(z)$ is an excellent one for many ferroelectric materials, where P is of the order of $0.1–1\,\mathrm{C/m^2}$ and $D - P = \epsilon_0 \mathcal{E}$ is typically much smaller than $10^{-3}\,\mathrm{C/m^2}$. Thus, assuming $D(z) \sim P(z)$ entails errors of 1% or less.[22] Moreover, the $SrTiO_3$ spacer becomes polarized so as to minimize the polarization mismatch with the contiguous $PbTiO_3$ layers, thereby recompensing the energetic cost of the coupling of the depolarization field and polarization at the interface.

Independently of the sign of the external fractional charge, the rumpling parameter at the free PbO surface is essentially the same [Fig. 2(b)]. This is the region where the largest atomic relaxations are located with the alchemical atom moving outward (toward the vacuum region) and the metal ion relaxing inward (toward the interior of the neighbor $PbTiO_3$ layer). The sign and magnitude are essentially the same as the one obtained for a PbO-terminated free-standing $PbTiO_3$ slab.[36] Then, the rumpling parameter follows an oscillatory pattern till it converges, around two unit cells away from the free surface, to a constant value within the insulating layers that is determined by the value of D. At the interface between $PbTiO_3$ and $SrTiO_3$, there is an interface dipole produced by an intrinsic rumpling (present even for $D = 0$), which superposes to that determined by the macroscopic displacement field. In a sequence like

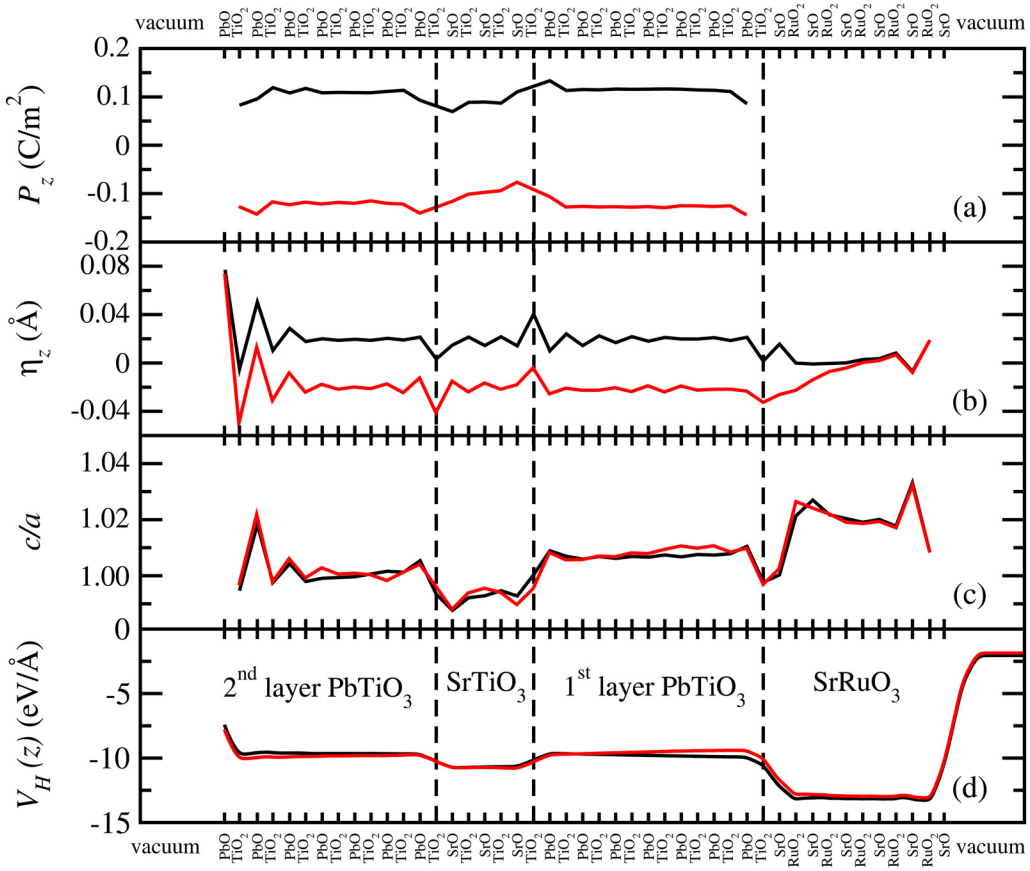

FIG. 2. Layer-by-layer polarization (a), rumpling parameter (b), tetragonality (c), and profile of the smoothed electrostatic potential energy for a slab with $Q = \pm 0.10e$ ($D = 1.866 \times 10^{-3}\,\mathrm{e/Bohr^2} = 0.107\,\mathrm{C/m^2}$). Black (respective red) lines represent the positive (respective negative) value of D. Dashed vertical lines delimit the regions of the different layers.

TABLE I. Continuity of the displacement field D in the dielectric layers of the slab from the computed layer-by-layer polarization P and the macroscopic electric field $\mathcal{E}$. The nominal external fractional charge is $Q = 0.10$, which corresponds to a nominal $D = 0.1067$ C/m^2.

	P (C/m^2)	$\mathcal{E}$ (MV/m)	D (C/m^2)
First $PbTiO_3$ layer	0.108	−132.413	0.106
$SrTiO_3$ layer	0.106	126.912	0.107
Second $PbTiO_3$ layer	0.103	−36.0503	0.102

PbO–TiO_2–SrO (respectively, SrO–TiO_2–PbO), the Ti atom always moves toward the PbO layer, producing a negative (respectively, positive) rumpling at the corresponding interface, as clearly shown in Fig. 2(b). Finally, the rumpling parameter decays within $SrRuO_3$ and vanishes in the interior of the metal electrode.

Regarding the interplanar distance and tetragonality, displayed in Fig. 2(c), the behavior is largely independent of the direction of the polarization. In both cases, the surface layer contracts substantially inward (toward the bulk of the material). This fact can be related with the tendency to strength the remaining bonds at the free-standing slab by reducing the distance between neighbor atoms. This effect, present even in the unpolarized slab ($D = 0$), superposes to the polarization-strain coupling that tends to expand the unit cell along the z-direction. Then, the change in the interlayer distance induced by the presence of a free surface displays a similar oscillatory behavior as the one discussed for the rumpling (decrease of the interlayer distance between the first and second layers, expansion between the second and the third, and a reduction again between the third and the fourth), although its magnitude reduces when we move toward the interior of the material. As a consequence, the total tetragonality (sum of the effects of the polarization-induced and surface-induced change in the out-of-plane lattice constant) is smaller than one for the unit cell at the surface (surface-induced contraction wins over the polarization-induced expansion), increases abruptly for the second-unit cell (both effects cooperate to make the unit cell larger along z), and follows the oscillatory behavior seen in Fig. 2(c) for the $PbTiO_3$ layer in between the vaccum and the spacer (labeled as a second $PbTiO_3$ layer in Fig. 1). For the $PbTiO_3$ layer in between the $SrTiO_3$ spacer and the $SrRuO_3$ electrode (labeled as a first $PbTiO_3$ layer in Fig. 1), the effect of the surface has totally disappeared, and the only contribution is the polarization-induced expansion that tends to increase c/a.

The behavior of the $SrTiO_3$ layer is peculiar. On the one hand, we expect to have a tetragonality larger than one due to the induced-polarization seen in Fig. 2(a). On the other hand, there is chemical pressure on the spacer due to its proximity with $PbTiO_3$: as we shall discuss below, the TiO_2 layer in between PbO and SrO behaves more like $PbTiO_3$ than $SrTiO_3$, and it pushes the $SrTiO_3$ layer from both sides due to the stronger tendency of $PbTiO_3$ to expand. As a consequence, we observe the counterintuitive effect that $c/a < 1$ in $SrTiO_3$. Only for larger thicknesses of this spacing layer, we would observe the tendency to recover the polarization-strain coupling expansion. $SrRuO_3$ is expanded due to the mechanical effect induced by the in-plane epitaxial contraction.

Finally, from the derivative of the profile of the nanosmoothed average[44] of the electrostatic potential energy shown in Fig. 2(d), we have access to the internal electric field within the different layers of the material, $\mathcal{E}$. If we sum the polarization at the center of the different dielectric layers shown in Fig. 2(a) with the local value of $\epsilon_0\mathcal{E}$, we arrive to the expected result that the out-of-plane component of the electric displacement D field is constant throughout the dielectric layers of the slab. Numerically, this is double-checked for the slab with a nominal external fractional charge of $Q = +0.10$

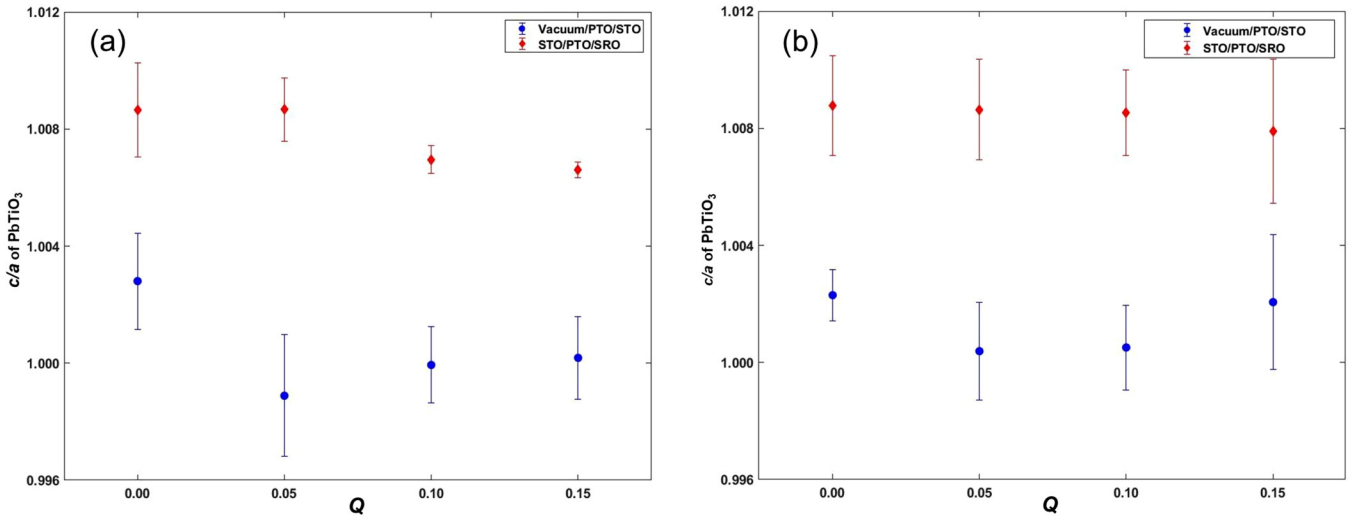

FIG. 3. Tetragonality of the $PbTiO_3$ layers as a function of the external fractional charge Q for (a) positive external charges and (b) negative external charges. Red diamonds represent average c/a taken over all the layers of the first $PbTiO_3$ layer (between the $SrTiO_3$ spacer and the $SrRuO_3$ electrode), while blue squares correspond to the second $PbTiO_3$ layer (between the $SrTiO_3$ spacer and vacuum). The error bars are the sample standard deviation.

($D = 0.1067\ \mathrm{C/m^2}$) in Table I. Only a small deviation is found for the $PbTiO_3$ layer closer to the free surface due to the interplay with the surface-induced relaxation, which makes more difficult for the local polarization to achieve a constant well-defined value.

As it is clear from the previous discussion, the different chemical environment of the two $PbTiO_3$ layers produces a slightly different behavior that translates into a different tetragonality c/a. In Fig. 3, we display c/a at the center of the two $PbTiO_3$ layers for different external fractional charges. This difference in tetragonality between the two layers is in qualitatively good agreement with the experimental findings of Ref. 20. A quantitative comparison is not possible due to the impossibility of doping our slabs with large fractional charge without avoiding the appearance of spurious transfer of charge between the metallic electrode and the bottom of the conduction bands of the dielectric layers.[22] For the first $PbTiO_3$ layer (between the $SrTiO_3$ spacer and the $SrRuO_3$ electrode), the tetragonality is almost constant, independent of the value of Q. This is in good agreement with the bulk calculations by Bonini *et al.*[45] where, within this regime of electric displacements, the out-of-plane lattice constant of bulk $PbTiO_3$ does not change appreciably (see the top panel of Fig. 1 of Ref. 45). For the second $PbTiO_3$ layer (between the $SrTiO_3$ spacer and vacuum), the average tetragonality drops from the undoped system to the charged configuration with $Q = \pm 0.05$ and then progressively increases with the external charge, as the polarization-induced effect become more dominant over the surface-induced influence.

B. Electronic structure

Figure 4 shows the layer (spatially) resolved projected density of states (PDOS) on all the atomic orbitals of a given ABO_3 unit cell (A = Sr or Pb, and B = Ti or Ru, depending on the layer). All the PDOS curves were calculated following the recipe given in Sec. III A 1 of Ref. 22 with the Dirac delta functions for the eigenvalues in the PDOS computations replaced by smearing normalized Gaussians with a finite width that is twice as large, as suggested in

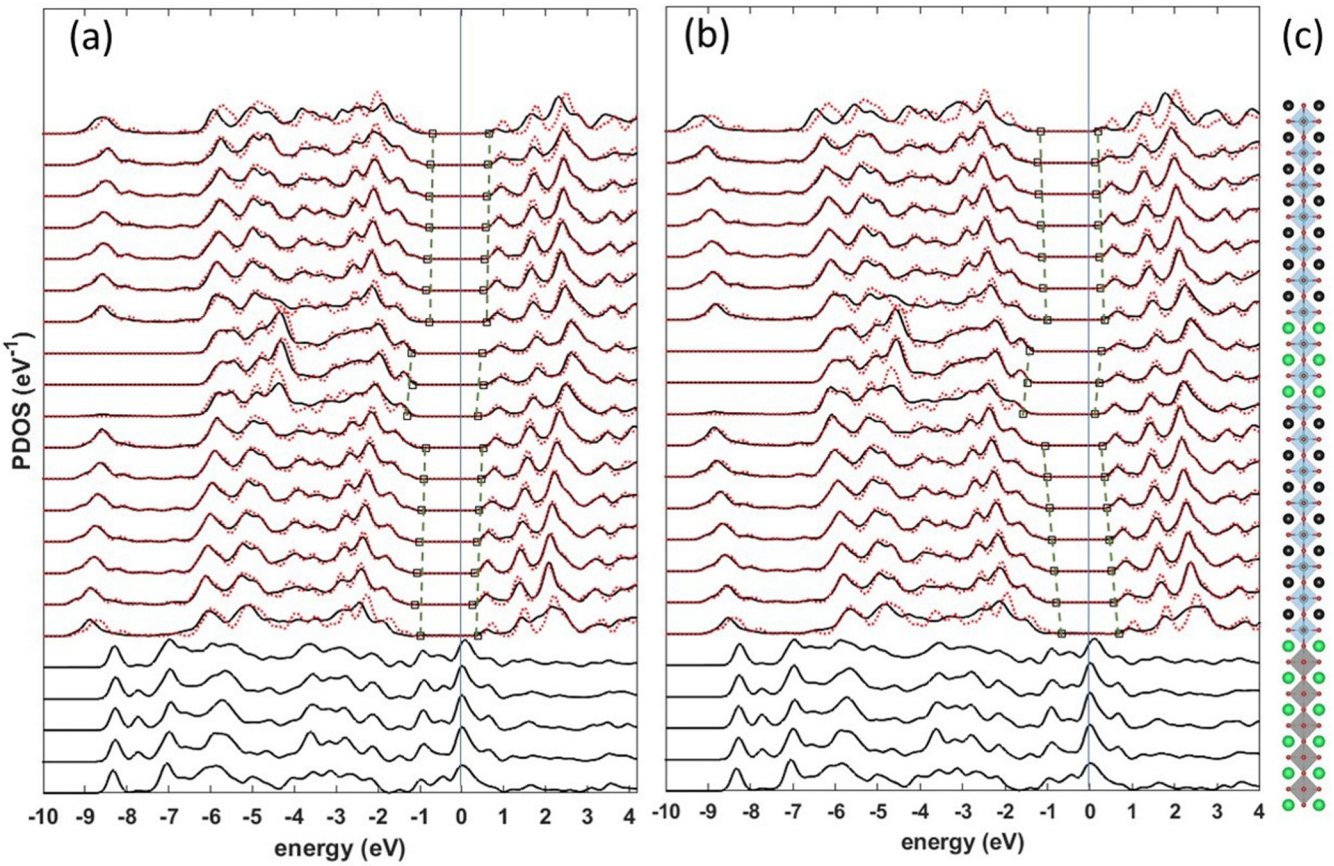

FIG. 4. Layer-by-layer PDOS on the atoms at the different ABO_3 unit cells (A = Sr or Pb, and B = Ti or Ru, depending on the layer) for (a) $Q = +0.10$ and (b) $Q = -0.10$. Each panel represents the PDOS on the corresponding unit cell located at the same height in panel (c). The bulk PDOS curves (red dashed) are aligned to match the Ti(3*s*) peak. The squares represent the position of the local band edges, computed following the recipe of Ref. 22. The dashed black lines are a linear interpolation of calculated band edges. The Fermi level is located at zero energy, as marked by the vertical blue line.

Appendix B of Ref. 22. On top of the heterostructure PDOS, we superimpose the bulk PDOS (dashed red lines), calculated with an equivalent k-point sampling. The bulk reference calculation was computed from a periodic bulk calculation with a five-atom per unit cell $PbTiO_3$ or $SrTiO_3$ structure with the atomic distortions and out-of-plane strain extracted from a region of the heterostructure where the relaxed atomic configuration (Fig. 1) has converged into a regular pattern. Finally, we note that the superposition of the bulk PDOS and supercell PDOS at each layer was done by matching the sharp peaks of the Ti($3s$) semicore band.

As it is clearly seen in Fig. 4, the surface PbO layer is locally insulating (no PDOS at the Fermi energy), validating the use of the fractional external charges to constraint the electric displacement field.

For the small values of Q used in this work, the Schottky barriers between the first $PbTiO_3$ layer and the Fermi level of the metallic electrode are well behaved with the bottom of the conduction band of the dielectric layers above the Fermi level of the metal electrode. We have not observed a spurious transfer of charge from $SrRuO_3$ to the bottom of the conduction band of the ferroelectric due to the bandgap underestimation inherent to the LDA. The pathological behavior appears when $Q \geq 0.15$, first observed in the structures negatively doped, i.e., with an alchemical atom mixing O and N.

Within the dielectric layers, a well-defined energy gap persists in all layers between the top of the valence bands (mostly O-$2p$ character) and the bottom of the conduction bands (mostly Ti-t_{2g} in character). The PDOS in each layer appears rigidly shifted with respect to the neighboring two layers, consistent with the presence of an internal electric field, whose value is consistent with that reported in Table I.

The electronic structure of the unit cell at the interface between the $PbTiO_3$ and the $SrTiO_3$ spacing layers resembles more to the one in the Pb-based perovskite, a fact that was used above to justify the chemical pressure felt by the spacer layer.

IV. CONCLUSIONS

Using state of the art first-principles calculations, where we have been able to carefully control the electrical, mechanical, and chemical boundary conditions of a complex oxide heterostructure, we have clearly identified how the final structure comes from a delicate balance between all of these interactions. For the $PbTiO_3$ layer in between the $SrTiO_3$ spacer and vacuum, there is a compromise between the oscillatory behavior imposed by the surface-induced relaxation and the homogeneous ferroelectric displacement patterns coming from the finite electric field displacement. In the $PbTiO_3$ layer in between the $SrTiO_3$ spacer and the $SrRuO_3$ electrode, the surface effects are negligible and only the ferroelectric distortions survive. The behavior of the $SrTiO_3$ spacing layer is determined on the one hand by the requirement to polarize it in order to minimize the polarization mismatch with the adjacent $PbTiO_3$ layers and to preserve the value of D, while on the other hand, there is a chemical pressure imposed by the neighbor ferroelectric layers.

Unfortunately, a quantitative comparison with the experimental results of Ref. 20 is not possible because for large enough values of D, the slab becomes pathological from the computational point of view with a spurious transfer of charge from the metallic electrode to the bottom of the conduction band of the ferroelectric layers. This failure cannot be alleviated by the use of LDA+U since the Hubbard term increases the bandgap but it kills the polarization due to the reduction of the Ti-$3d$-O-$2p$ hybridization. A very promising avenue has been opened by the recently developed general-purpose strongly constrained and appropriately normed (SCAN) meta-GGA functional,[46,47] which has been shown to systematically improve over LDA/PBE for geometries and energies of different bonding materials. Finally, another interesting research line is the simulation of the domain structures, a challenge for the first-principles simulations due to the large size of the simulation box required.

ACKNOWLEDGMENTS

R.M. thanks Professor Emily Hilder and Professor Nikki Stanford for their support. J.J. acknowledges financial support from the Spanish Ministry of Science, Innovation and Universities through Grant No. PGC2018-096955-B-C41. The authors also gratefully acknowledge the computer resources, technical expertise, and assistance provided by the NCI National Facility in Canberra, Australia, which is supported by the Australian Commonwealth Government. The authors also acknowledge the computational resources provided by Intersect Australia Ltd.

DATA AVAILABILITY

The data that support the findings of this study are available within the article.

REFERENCES

[1]P. Zubko, S. Gariglio, M. Gabay, P. Ghosez, and J.-M. Triscone, "Interface physics in complex oxide heterostructures," Annu. Rev. Condens. Matter Phys. **2**, 141 (2011).
[2]S. Ismail-Beigi, F. J. Walker, A. S. Disa, K. M. Rabe, and C. H. Ahn, "Picoscale materials engineering," Nat. Rev. Mater. **2**, 17060 (2017).
[3]H. Wang, F. Tang, P. H. Dhuvad, and X. Wu, "Interface enhanced functionalities in oxide superlattices under mechanical and electric boundary conditions," npj Comput. Mater. **6**, 52 (2020).
[4]Q. Zhang, E. M. Dufresne, P. Chen, J. Park, M. P. Cosgriff, M. Yusuf, Y. Dong, D. D. Fong, H. Zhou, Z. Cai, R. J. Harder, S. J. Callori, M. Dawber, P. G. Evans, and A. R. Sandy, "Thermal fluctuations of ferroelectric nanodomains in a ferroelectric-dielectric $PbTiO_3/SrTiO_3$ superlattice," Phys. Rev. Lett. **118**, 097601 (2017).
[5]P. Chen, M. P. Cosgriff, Q. Zhang, S. J. Callori, B. W. Adams, E. M. Dufresne, M. Dawber, and P. G. Evans, "Field-dependent domain distortion and interlayer polarization distribution in $PbTiO_3/SrTiO_3$ superlattices," Phys. Rev. Lett. **110**, 047601 (2013).
[6]E. Bousquet, M. Dawber, N. Stucki, C. Lichtensteiger, P. Hermet, S. Gariglio, J.-M. Triscone, and P. Ghosez, "Improper ferroelectricity in perovskite oxide artificial superlattices," Nature **452**, 732 (2008).
[7]P. Aguado-Puente, P. García-Fernández, and J. Junquera, "Interplay of couplings between antiferrodistortive, ferroelectric, and strain degrees of freedom in monodomain $PbTiO_3/SrTiO_3$ superlattices," Phys. Rev. Lett. **107**, 217601 (2011).
[8]P. Aguado-Puente and J. Junquera, "Structural and energetic properties of domains in $PbTiO_3/SrTiO_3$ superlattices from first principles," Phys. Rev. B **85**, 184105 (2012).

[9]P. Zubko, N. Jecklin, A. Torres-Pardo, P. Aguado-Puente, A. Gloter, C. Lichtensteiger, J. Junquera, O. Stéphan, and J.-M. Triscone, "Electrostatic coupling and local structural distortions at interfaces in ferroelectric/paraelectric superlattices," Nano Lett. **12**, 2846 (2012).
[10]M. Dawber, N. Stucki, C. Lichtensteiger, S. Gariglio, P. Ghosez, and J.-M. Triscone, "Tailoring the properties of artificially layered ferroelectric superlattices," Adv. Mater. **19**, 4153 (2007).
[11]E. D. Specht, H.-M. Christen, D. P. Norton, and L. A. Boatner, "X-ray diffraction measurement of the effect of layer thickness on the ferroelectric transition in epitaxial $KTaO_3/KNbO_3$ multilayers," Phys. Rev. Lett. **80**, 4317 (1998).
[12]A. K. Yadav, C. T. Nelson, S. L. Hsu, Z. Hong, J. D. Clarkson, C. M. Schlepütz, A. R. Damodaran, P. Shafer, E. Arenholz, L. R. Dedon, D. Chen, A. Vishwanath, A. M. Minor, L. Q. Chen, J. F. Scott, L. W. Martin, and R. Ramesh, "Observation of polar vortices in oxide superlattices," Nature **530**, 198 (2016).
[13]P. Zubko, J. C. Wojdel, M. Hadjimichael, S. Fernandez-Pena, A. Sené, I. Luk'yanchuk, J.-M. Triscone, and J. Íñiguez, "Negative capacitance in multidomain ferroelectric superlattices," Nature **534**, 524 (2016).
[14]A. K. Yadav, K. X. Nguyen, Z. Hong, P. García-Fernández, P. Aguado-Puente, C. T. Nelson, S. Das, B. Prasad, D. Kwon, S. Cheema, A. I. Khan, C. Hu, J. Íñiguez, J. Junquera, L.-Q. Chen, D. A. Muller, R. Ramesh, and S. Salahuddin, "Spatially resolved steady-state negative capacitance," Nature **565**, 468 (2019).
[15]P. Shafer, P. García-Fernández, P. Aguado-Puente, A. R. Damodaran, A. K. Yadav, C. T. Nelson, S.-L. Hsu, J. C. Wojdeł, J. Íñiguez, L. W. Martin, E. Arenholz, J. Junquera, and R. Ramesh, "Emergent chirality in the electric polarization texture of titanate superlattices," Proc. Natl. Acad. Sci. U.S.A. **115**, 915 (2018).
[16]Q. Zhang, L. Xie, G. Liu, S. Prokhorenko, Y. Nahas, X. Pan, L. Bellaiche, A. Gruverman, and N. Valanoor, "Nanoscale bubble domains and topological transitions in ultrathin ferroelectric films," Adv. Mater. **29**, 1702375 (2017).
[17]Q. Zhang, S. Prokhorenko, Y. Nahas, L. Xie, L. Bellaiche, A. Gruverman, and N. Valanoor, "Deterministic switching of ferroelectric bubble nanodomains," Adv. Funct. Mater. **29**, 1808573 (2019).
[18]S. Das, Y. L. Tang, Z. Hong, M. A. P. Gonçalves, M. R. McCarter, C. Klewe, K. X. Nguyen, F. Gómez-Ortiz, P. Shafer, E. Arenholz, V. A. Stoica, S.-L. Hsu, B. Wang, C. Ophus, J. F. Liu, C. T. Nelson, S. Saremi, B. Prasad, A. B. Mei, D. G. Schlom, J. Íñiguez, P. García-Fernández, D. A. Muller, L. Q. Chen, J. Junquera, L. W. Martin, and R. Ramesh, "Observation of room-temperature polar skyrmions," Nature **568**, 368 (2019).
[19]C. Lichtensteiger, S. Fernandez-Pena, C. Weymann, P. Zubko, and J.-M. Triscone, "Tuning of the depolarization field and nanodomain structure in ferroelectric thin films," Nano Lett. **14**, 4205 (2014).
[20]G. Liu, J. Chen, C. Lichtensteiger, J.-M. Triscone, P. Aguado-Puente, J. Junquera, and N. Valanoor, "Positive effect of an internal depolarization field in ultrathin epitaxial ferroelectric films," Adv. Electron. Mater. **2**, 1500288 (2016).
[21]C. Lichtensteiger, "*InteractiveXRDFit*: A new tool to simulate and fit x-ray diffractograms of oxide thin films and heterostructures," J. Appl. Crystallogr. **51**, 1745 (2018).
[22]M. Stengel, P. Aguado-Puente, N. A. Spaldin, and J. Junquera, "Band alignment at metal/ferroelectric interfaces: Insights and artifacts from first principles," Phys. Rev. B **83**, 235112 (2011).
[23]J. Íñiguez, P. Zubko, I. Luk'yanchuk, and A. Cano, "Ferroelectric negative capacitance," Nat. Rev. Mater. **4**, 243 (2019).
[24]D. M. Ceperley and B. J. Alder, "Ground state of the electron gas by a stochastic method," Phys. Rev. Lett. **45**, 566 (1980).
[25]P. Hohenberg and W. Kohn, "Inhomogeneous electron gas," Phys. Rev. **136**, B864 (1964).
[26]W. Kohn and L. J. Sham, "Self-consistent equations including exchange and correlation effects," Phys. Rev. **140**, A1133 (1965).
[27]J. M. Soler, E. Artacho, J. D. Gale, A. García, J. Junquera, P. Ordejón, and D. Sánchez-Portal, "The SIESTA method for *ab initio* order-n materials simulation," J. Phys. Condens. Matter **14**, 2745 (2002).
[28]N. Troullier and J. L. Martins, "Efficient pseudopotentials for plane-wave calculations," Phys. Rev. B **43**, 1993 (1991).
[29]L. Kleinman and D. M. Bylander, "Efficacious form for model pseudopotentials," Phys. Rev. Lett. **48**, 1425 (1982).
[30]O. F. Sankey and D. J. Niklewski, "*Ab initio* multicenter tight-binding model for molecular-dynamics simulations and other applications in covalent systems," Phys. Rev. B **40**, 3979 (1989).
[31]E. Artacho, D. Sánchez-Portal, P. Ordejón, A. García, and J. M. Soler, "Linear-scaling ab-initio calculations for large and complex systems," Phys. Status Solidi B **215**, 809 (1999).
[32]J. Junquera, M. Zimmer, P. Ordejón, and P. Ghosez, "First-principles calculation of the band offset at $BaO/BaTiO_3$ and $SrO/SrTiO_3$ interfaces," Phys. Rev. B **67**, 155327 (2003).
[33]J. Sifuna, P. García-Fernández, G. S. Mayali, G. Amolo, and J. Junquera, "First-principles study of two-dimensional electron and hole gases at the head-to-head and tail-to-tail 180° domain walls in $PbTiO_3$ ferroelectric thin films," Phys. Rev. B **101**, 174114 (2020).
[34]M. Verissimo-Alves, P. García-Fernández, D. I. Bilc, P. Ghosez, and J. Junquera, "Highly confined spin-polarized two-dimensional electron gas in $SrTiO_3/SrRuO_3$ superlattices," Phys. Rev. Lett. **108**, 107003 (2012).
[35]H. J. Monkhorst and J. D. Pack, "Special points for brillouin-zone integrations," Phys. Rev. B **13**, 5188 (1976).
[36]B. Meyer, J. Padilla, and D. Vanderbilt, "Theory of $PbTiO_3$, $BaTiO_3$, and $SrTiO_3$ surfaces," Faraday Discuss. **114**, 395 (1999).
[37]L. Bengtsson, "Dipole correction for surface supercell calculations," Phys. Rev. B **59**, 12301 (1999).
[38]B. Meyer and D. Vanderbilt, "*Ab initio* study of $batio_3$ and $pbtio_3$ surfaces in external electric fields," Phys. Rev. B **63**, 205426 (2001).
[39]M. Stengel and D. Vanderbilt, "Berry-phase theory of polar discontinuities at oxide-oxide interfaces," Phys. Rev. B **80**, 241103 (2009).
[40]M. Stengel, "First-principles modeling of electrostatically doped perovskite systems," Phys. Rev. Lett. **106**, 136803 (2011).
[41]L. Bellaiche and D. Vanderbilt, "Virtual crystal approximation revisited: Application to dielectric and piezoelectric properties of perovskites," Phys. Rev. B **61**, 7877 (2000).
[42]R. Poloni, J. Íñiguez, A. García, and E. Canadell, "An efficient computational method for use in structural studies of crystals with substitutional disorder," J. Phys. Condens. Matter **22**, 415401 (2010).
[43]M. Stengel, N. A. Spaldin, and D. Vanderbilt, "Electric displacement as the fundamental variable in electronic-structure calculations," Nat. Phys. **5**, 304 (2009).
[44]J. Junquera, M. H. Cohen, and K. M. Rabe, "Nanoscale smoothing and the analysis of interfacial charge and dipolar densities," J. Phys. Condens. Matter **19**, 213203 (2007).
[45]J. Bonini, J. W. Bennett, P. Chandra, and K. M. Rabe, "First-principles bulk-layer model for dielectric and piezoelectric responses in superlattices," Phys. Rev. B **99**, 104107 (2019).
[46]Y. Zhang, J. Sun, J. P. Perdew, and X. Wu, "Comparative first-principles studies of prototypical ferroelectric materials by LDA, GGA, and SCAN meta-GGA," Phys. Rev. B **96**, 035143 (2017).
[47]J. Sun, R. Remsing, Y. Zhang, Z. Sun, A. Ruzsinszky, H. Peng, Z. Yang, A. Paul, U. Waghmare, X. Wu, M. Klein, and J. Perdew, "Accurate first-principles structures and energies of diversely bonded systems from an efficient density functional," Nat. Chem. **8**, 831 (2016).